PAPER • OPEN ACCESS

Highly fluorescent nitrogen-doped graphene quantum dots (N-GQDs) synthesized from *Pennisetum purpureum* for selective and sensitive detection of Fe^{3+} ions

To cite this article: Fathah Dian Sari *et al* 2023 *Mater. Res. Express* **10** 075603

Materials Research Express

PAPER

Highly fluorescent nitrogen-doped graphene quantum dots (N-GQDs) synthesized from *Pennisetum purpureum* for selective and sensitive detection of Fe^{3+} ions

Fathah Dian Sari[1,2], **Chotimah**[3], **Roto**[1] **and Indriana Kartini**[1,*]

[1] Department of Chemistry, Faculty of Mathematics and Natural Sciences, Universitas Gadjah Mada, Sekip Utara BLS 21, Yogyakarta 55281, Indonesia
[2] Department of Pharmacy, Faculty of Science and Technology, Universitas PGRI Yogyakarta, Jl. PGRI I No. 117, Sonosewu, Yogyakarta 55182, Indonesia
[3] Department of Physics, Faculty of Mathematics and Natural Sciences, Universitas Gadjah Mada, Sekip Utara BLS 21, Yogyakarta 55281, Indonesia
* Author to whom any correspondence should be addressed.

E-mail: indriana@ugm.ac.id

Keywords: graphene quantum dots, ethylenediamine, biomass, doping, metal ion detection

OPEN ACCESS

RECEIVED
21 April 2023

REVISED
24 June 2023

ACCEPTED FOR PUBLICATION
12 July 2023

PUBLISHED
27 July 2023

Abstract

The synthesis of nitrogen-doped Graphene Quantum Dots (N-GQDs) employing *Pennisetum purpureum* (elephant grass) as the carbon precursor and ethylenediamine (EDA) as the nitrogen source was conducted. This study highlights the potential applications of nitrogen-doped multi-fluorescent graphene quantum dots (N-GQDs) in the detection of Fe^{3+}. The synthesized N-GQDs have been studied using UV–vis spectrophotometry, fluorescence spectrometry, Raman spectrometry, FT-IR spectrometry, x-ray spectroscopy, selected-area electron diffraction, transmission and high-transmission electron microscopy. The acquired N-GQDs were observed to have an almost hexagonal shape with a lateral size of 2.42 nm and exhibited a comparable quantum yield of approximately 26%. The N-GQDs that have been prepared with consistent size distribution and a significant amount of nitrogen and oxygen-based functional groups showcase outstanding water dispersity. The N-GQDs exhibited the capability to identify the Fe^{3+} ions in a broad range concentration of 1–600 μM by creating an N-GQDs-Fe^{3+} complex through the occurrence of functional groups like nitrogen, carbonyl, and carboxyl on N-GQDs surface, has a lower limit of detection at approximately 60 nM. Our study provides evidence that the N-GQDs produced a strong and persistent fluorescence, which is highly soluble in water, notably the precise and selective detection of Fe^{3+} in water-based solutions.

1. Introduction

Recent breakthroughs in nanotechnology have resulted in the discovery of Graphene Quantum Dots (GQDs), made of graphene sheets having smaller lateral sizes below 100 nm, and existing in single, double, or few-layer (not more than 10) configurations [1, 2]. The GQDs derived from carbon dots and graphene represent a recently discovered class of materials with exceptional chemical, structural, and electric properties and versatile optical characteristics such as photoluminescence and electroluminescence [3]. The GQDs have gained significant attention as a prospective fluorescence-based sensor applied for detecting metallic ions, biomolecules, and small molecules, through their exceptional material characteristics for instance water solubility, low toxicity, stable fluorescence, and eco-friendliness [4–6]. However, numerous investigations on GQDs concentrate solely on enhancing their optical properties and expanding their applications, often overlooking the critical aspect of sourcing carbon. Adopting a greener approach to fabricate high-quality GQDs remains a crucial issue that needs to be addressed urgently [7]. Using renewable, economical, and eco-friendly biomass resources satisfies the

immediate demand for high-volume production of biomass-derived GQDs and fosters sustainable application [8].

Grass, a part of biomass, is one of the potential carbon sources that can be utilized to synthesize GQDs [9]. The grass is particularly prolific and is a major component of solid green waste, which requires significant storage space and expensive management. Due to the presence of recalcitrant components, composting the grass waste is difficult and time-consuming. When the grass waste is not properly disposed of, it can accumulate and harm the environment. Therefore, the transformation of grass waste materials into valuable materials is highly demanding, particularly for use as the precursor in the GQDs synthesis [9, 10]. The formation of GQDs from the grass contains various functional groups, resulting in the formation of new energy levels and causing changes in the optical characteristics of GQDs [11, 12]. However, considering the advantages of their optical properties, the production and applications of GQDs were still limited by the lower luminescence efficiency due to the lower QY. Thus, necessitating modifications of the GQDs is highly desirable to improve the luminescence efficiency [11–13].

Several methods have been put forward to enhance the luminescence properties of the GQDs. Surface passivation or functionalization is the widely used method to enhance the fluorescence characteristics of carbon nanodots in the beginning stages of synthesis by altering the surface emissive state of the precursor, particularly inert raw materials [14–17]. Another way to improve the luminescence efficiency is by using atomic doping. Here, the existence of doping including nitrogen (N) and sulfur (S) in the GQDs effectively elevate their optical and electrical properties owing to the presence of the degree of purity inside the band gap [18, 19]. Several numerous new types of GQDs have been reported, including nitrogen-doped GQDs (N-GQDs), sulfur-doped GQDs (S-GQDs), and N,S-co-doped GQDs (N,S-GQDs) [20–23]. However, understanding the fluorescence mechanism and its correlation to the enhancement intensity and quenching are needed to be further clarified. Therefore, this study aims to explore how the role of atomic doping on the fluorescence properties of the grass-based GQDs and discuss their possible application as metallic ion sensors.

This study reports the successful synthesis of N-GQDs possessing high crystallinity via a single-step hydrothermal approach using an elephant grass (*Pennisetum purpureum*) as a carbon precursor and ethylenediamine (EDA) for nitrogen doping. EDA is a frequently employed molecule to introduce nitrogen atom doping in order to passivate the surface of N-GQDs. The nitrogen atoms present in EDA undergo reactions with the functional groups located on the surface of GQDs, leading to the integration of nitrogen atoms into the lattice of graphene. This integration of nitrogen atoms introduces dopant atoms into the structure of graphene, subsequently altering its electronic properties specifically on the surface of N-GQDs [24]. The resulting N-GQDs exhibit excellent fluorescence properties having QY of approximately 26% that enable selective and responsive sensing of metallic ions. Utilizing the fluorescence response of N-GQDs, a fluorescence-based sensor was developed to detect Fe^{3+} ions. The findings indicate that N-GQDs were capable of detecting Fe^{3+} ions, resulting in quenching fluorescence. As per our understanding, most of the synthesis of carbon-based material from grass results in carbon nanodots with lower crystallinity, which is strongly different from our research. Therefore, our study provides further evidence for the industrial potential of N-GQDs, given their inexpensive starting materials, simple synthetic route, and high yield for practical applications.

2. Materials and methods

2.1. Materials

Elephant grass was gathered from a local farm situated in Yogyakarta, Indonesia. Merck supplied the following chemicals: $Al(NO_3)_3$, $Ca(NO_3)_2$, $CdSO_4$, $CoCl_2$, $CuCl_2$, $FeCl_3$, $FeSO_4$, KCl, $Pb(NO_3)_2$, $MnCl_2$, $Mg(NO_3)_2$, $HgCl_2$, NaCl, $NiCl_2$, $ZnCl_2$, HCl, NaOH, ethylenediamine (EDA), and quinine sulfate. Whatman 42 filter paper circles 55 mm were obtained from GE Healthcare. Deionized water (DI) was bought from CV. Progo Mulyo. No additional purification of the chemicals was necessary.

2.2. Experimental

2.2.1. Synthesis of N-GQDs

The process begins with crushing elephant grass (figure 1), and then the 1.0 g of dried grass is placed into a 25 ml stainless steel autoclave along with 0.05 ml EDA dispersed into a 10 ml measuring flask of DI, then heated to 180 °C for 6 h. After natural cooling to room temperature and allowing it to stand overnight, the light-brown solution underwent centrifugation for 15 min at 12000 rpm and was subjected to filtration using a Whatman membrane filter paper to remove impurities. The recovered supernatant was then partially freeze-dried to acquire a light-brown-colored dispersion for further characterization (see figure 1).

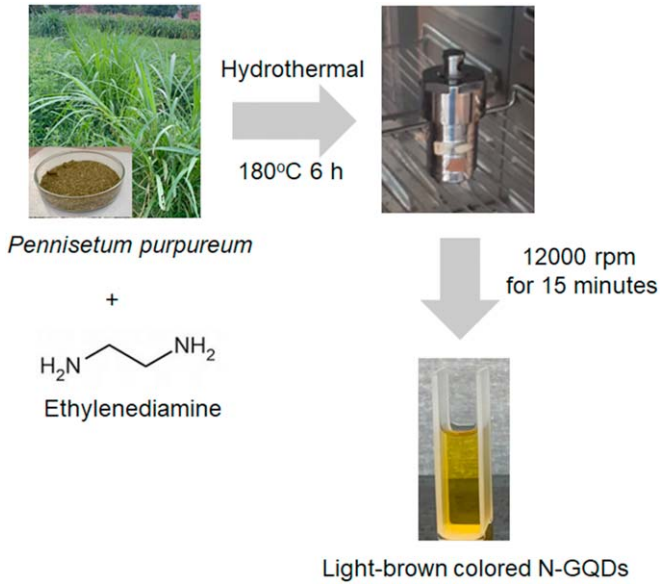

Figure 1. Schematic view of the one-step synthesis of N-GQDs.

2.2.2. pH-responsive fluorescence behavior of N-GQDs

The ability of N-GQDs to maintain stability across a diverse pH scale is crucial in sensing applications. In consequence, the emission intensity of N-GQDs in solutions of varying pH levels (2–12) was measured to determine the correlation between pH and fluorescence.

2.2.3. N-GQDs characterization

The N-GQDs sample's Ultraviolet-Visible (UV–vis) spectra were evaluated with a Thermo Scientific Genesys UV–vis spectrophotometer within the 200–600 nm wave range. Fourier-transform infrared (FT-IR) spectra extending from 500 to 4000 cm^{-1} were collected using a Thermo Scientific Nicolet iS-10 FT-IR spectrometer. The Shimadzu RF-600 spectrofluorometer was employed to measure the fluorescence spectra with a scan rate of 30000 nm min^{-1}. Raman Horiba hyperspectral spectroscopy with a 785 nm exciting laser, equipped with 600 nm gratings and a 10X VIS objective was used to conduct Raman spectra. The x-ray diffraction (XRD) analysis was executed using a Bruker D8 advance employing Cu Kα (0.154 nm), at room temperature (approximately 25 °C) over a 2θ range of 5°–60° with a scanning speed of 3/min. Transmission electron microscope (TEM) images were accomplished with JEOL JEM-1400 TEM microscopy with UC-A on Lacey 400 mesh Cu. A Tecnai D2360 Super Twin microscope was utilized to generate high-resolution transmission electron microscope images (HR-TEM). The instrument was operated with an acceleration voltage of 200 kV.

2.2.4. The detection of Fe^{3+} using N-GQDs

To assess the sensitivity of the N-GQDs sensor, the intensity of fluorescence was recorded at different Fe^{3+} concentrations, spanning from 0 to 600 μM, having previously determined the selectivity of N-GQDs. The N-GQDs's sensor selectivity was determined by analyzing the fluorescence spectra of various metal ions solutions (Na^{+}, Mg^{2+}, Al^{3+}, K^{+}, Ca^{2+}, Mn^{2+}, Fe^{2+}, Fe^{3+}, Co^{2+}, Ni^{2+}, Cu^{2+}, Zn^{2+}, Cd^{2+}, Hg^{2+}, and Pb^{2+}) and comparing them to the quenching of the fluorescence spectra at room temperature. To prepare for this analysis, a standard solution was then taken, and the fluorescence was measured after a 5-minute incubation period at ambient temperature. An excitation wavelength of 370 nm and a scan speed of 30000 nm min^{-1} was utilized for the measurements. The selectivity investigation of N-GQDs against several metal ions was conducted by adding 0.1 ml N-GQDs into the mixture of metal ions at a concentration of 600 μM and incubating for 5 min. The fluorescence spectra were recorded with a spectrofluorometer to determine whether other metal ions had a significant effect on the fluorescence intensity of N-GQDs so that the selective response of N-GQDs fluorescence to Fe^{3+} could be determined.

2.2.5. Quantum yield (QY) measurement

The fluorescence intensity in an aqueous dispersion was quantified to determine the QY of the N-GQDs using the methodology outlined by Atchudan *et al* (2018) in equation (1)[36].

$$QY_{N-GQDs} = QY_R \frac{I_{N-GQDs}}{I_R} \frac{A_R}{A_{N-GQDs}} \frac{\eta^2_{N-GQDs}}{\eta^2_R}, \quad (1)$$

where $QY_{N\text{-}GQDs}$ and QY_R are the fluorescence QY of the N-GQDs and the reference substance (quinine sulfate), respectively. $I_{N\text{-}GQDs}$ and I_R represent the fluorescence spectra of the N-GQDs and the reference substance, respectively. $A_{N\text{-}GQDs}$ represent the UV-visible absorption intensity of the N-GQDs, while A_R corresponds to the absorption intensity of the reference substance. The refractive index of the solvent used for the N-GQDs is indicated as $\eta_{N\text{-}GQDs}$, and the refractive index of the reference substance is denoted as η_R. The optical densities were determined using the Thermo Scientific Genesys UV-visible spectrophotometer. The reference material utilized was quinine sulfate dissolved in 0.1 M H_2SO_4 (with a literature QY of 0.54 at 360 nm). By maintaining an absorbance value below 0.10 during excitation at a wavelength of 360 nm, the re-absorption effects within the 10 mm fluorescence cuvette can be minimized.

3. Results and discussion

3.1. Characterization of the synthesized N-GQDs

The XRD pattern of synthesized N-GQDs as displayed in figure 2(a), exhibits three distinct scattering peaks at 28.39°, 40.68°, and 50.38°, which correspond to the (002), (101), and (004) planes of 2D graphene's hexagonal lattice (JCPDS 75–1621) along with the small amount of cubic phase (210), (220), (300) (JCPDS 18–0311) and cyclohexane monoclinic (011), (2'11), (221) (JCPDS file 48–1960), revealing the crystallinity structure of the N-GQDs. Additionally, the intense diffraction peak at $2\theta = 28.39°$ with high intensity and an interlayer spacing of 0.2 nm suggest that there is no steric hindrance in the basal plane, resulting in a tight packing arrangement akin to bulky graphite. These characteristics facilitate the creation of a graphene structure with minimal imperfections and a high level of crystallinity during the thermal conversion of carbon (carbonization) [5]. The lattice spacing in the (101) direction observed in the XRD, which was 0.2 nm, was found to agree with the HR-TEM images as illustrated in figures 2(b)–(c) [25]. This indicates that both the in-plane lattice in the (101) direction and the interlayer spacing in the (002) direction are present in GQDs. The XRD pattern indicated a less intense and broad peak in the (002) plane that shifted toward a lower angle of 2θ. The synthesized N-GQDs show that they are relatively small in size, as evidenced by figure 2(b) [5].

The HR-TEM picture of N-GQDs exhibited distinguished lattice fringes featuring an average in-plane 0.2 nm crystal spacing (figure 2(c)) in agreement with the (101) plane of graphite crystal [26], thereby providing additional confirmation of the layered structure of N-GQDs. The above findings confirm the occurrence of graphitization in the synthesis of N-GQDs. Electron diffraction patterns and TEM imaging were capable of being matched to the faultless hexagonal pattern (figures 2(b)–(c)) of graphene layers arranged in AB Bernal configuration within the hexagonal core with a spacing of 0.2 nm [27]. The SAED pattern (inset figure 2(b)) indicates the absence of supplementary diffraction peaks, implying that the domain does not contain rotational stacking faults, which are often observed in turbo static graphite [27, 28]. Furthermore, statistical analysis of the TEM image (figure 2(d)) reveals a Gaussian size distribution having a lateral dimension from 1.0–3.0 nm. The average lateral size is 2.42 nm, confirming the N-GQDs's uniform and homogenously dispersed properties. These results prove that the N-GQDs synthesized possess a structure characteristic of graphite, as previously reported [29–31].

Raman spectra obtained from the synthesized N-GQDs are presented in figure 2(e) and exhibit two wide signals: D-band centered at 1340 cm^{-1} and G-band located at 1560 cm^{-1}, as previously reported by Wang *et al* (2020) [21]. The presence of defects in the graphite lattice is reflected by the D-band, including the dangling bonds of carbon networks comprising sp^3-hybridized atoms. Meanwhile, the oscillation of sp^2-hybridized carbon atoms ordered in a 2D hexagonal arrangement is indicated by G-band, as explained by Krishnaiah *et al* (2022) [32]. The Raman spectra of N-GQDs also exhibit features resembling a reduced form of graphene oxide (RGO) as indicated by the presence of a peak in the 1600 cm^1 region which is the character of in-plane mode graphene, peaks at 1800–2200 cm^{-1} which is indicated out of plane modes, and a peak in the 2744 cm^{-1} region which indicates a few layers of wrinkled graphene [33, 34]. This result is in line with the TEM analysis in figures 2(b)–(c).

To assess the surface functionalization of N-GQDs, ATR-FTIR spectroscopy was carried out. The resulting ATR-FTIR spectrum (figure 2(f)) demonstrates a wide peak at 3000–3500 cm^{-1}, which can be contributed to the O-H functional groups exhibiting stretching vibrations that involved physically absorbed water molecules (H-O-H) and N-H found on the N-GQDs surface [11, 12, 15, 32, 35]. The stretching vibrations of symmetric and asymmetric C-H were identified by the peaks observed at 2835 and 2976 cm^{-1}, respectively. Furthermore, the bands at 1583, 1450, 1306, and 1068 cm^{-1} are indicative of C = C, C-N, COO^-, and C-O-C/C-N stretching vibrations, respectively [8, 15, 36, 37]. The identification of nitrogen-containing functional groups in N-GQDs was confirmed by the detection of characteristic peaks at 1450 cm^{-1} and 1211 cm^{-1}, associated with the

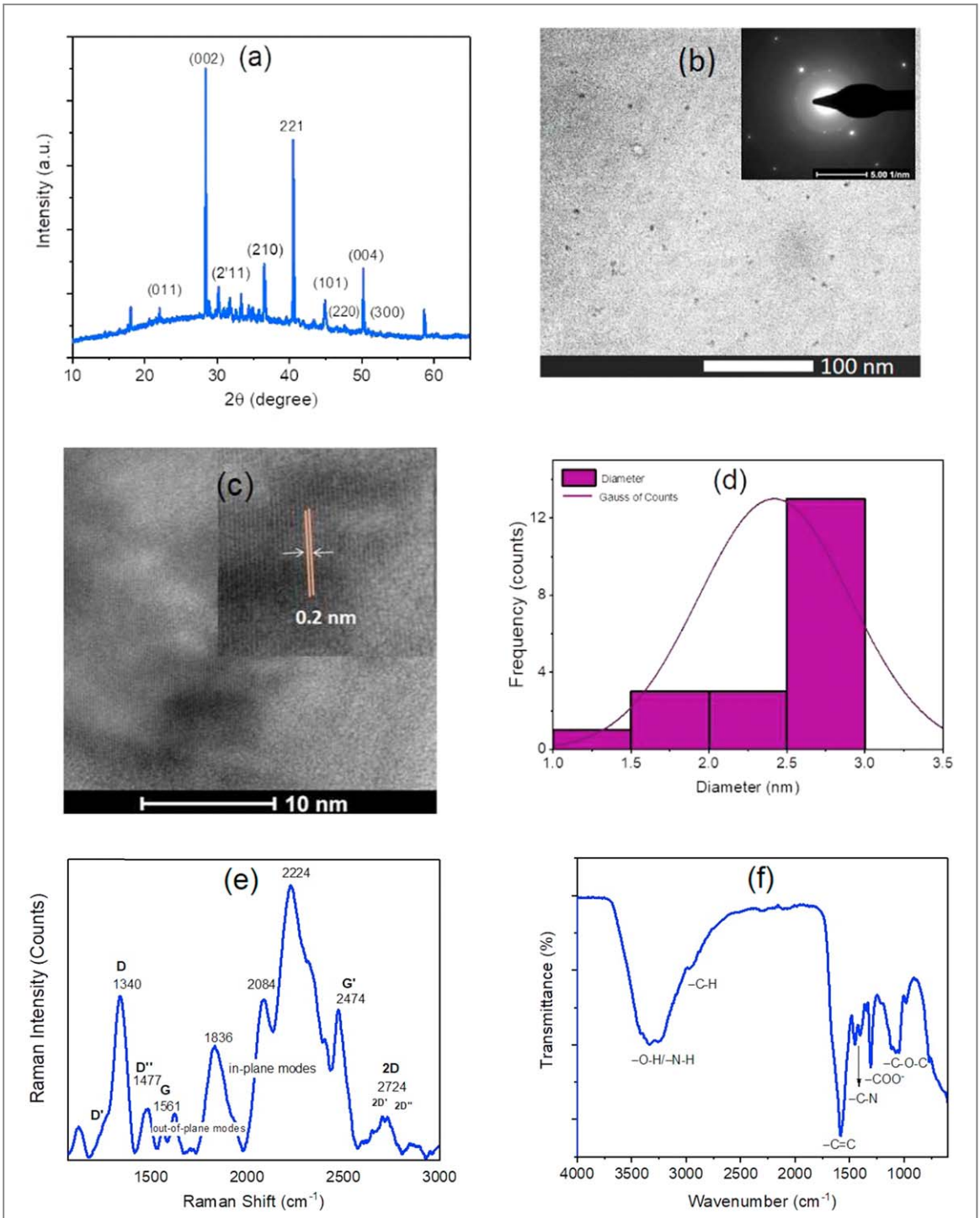

Figure 2. (a) X-Ray diffraction pattern, (b) TEM image with SAED inset picture, (c) N-GQDs interlayer spacing, (d) Distribution of particle size, (e) Raman spectra for N-GQDs, (f) FTIR spectra for synthesized N-GQDs.

stretching modes of C-N-C heterocyclic and C-N bond, respectively, based on previous research finding [15, 16, 38, 39]. The findings confirmed that the hydrothermal process involving a combination of ethylenediamine and elephant grass resulted in the formation of nitrogen-containing functional groups. As a result, nitrogen species were accurately introduced into the matrix of N-GQDs.

The solubility of N-GQDs in aqueous media is improved by the presence of functional groups, even without additional chemical modification. Additionally, the lack of significant stretching of amine groups (N-H) within the plane in the FTIR spectrum indicates the accomplished integration of nitrogen atoms within the N-GQDs. The ATR-FTIR analysis confirmed the occurrence of C, N, and O in the obtained N-GQDs, indicating that both C and N elements were derived from the precursors. The following is a hypothesized mechanism to produce N-GQDs via the synthesis process involving grass and ethylenediamine: since elephant grass is rich in

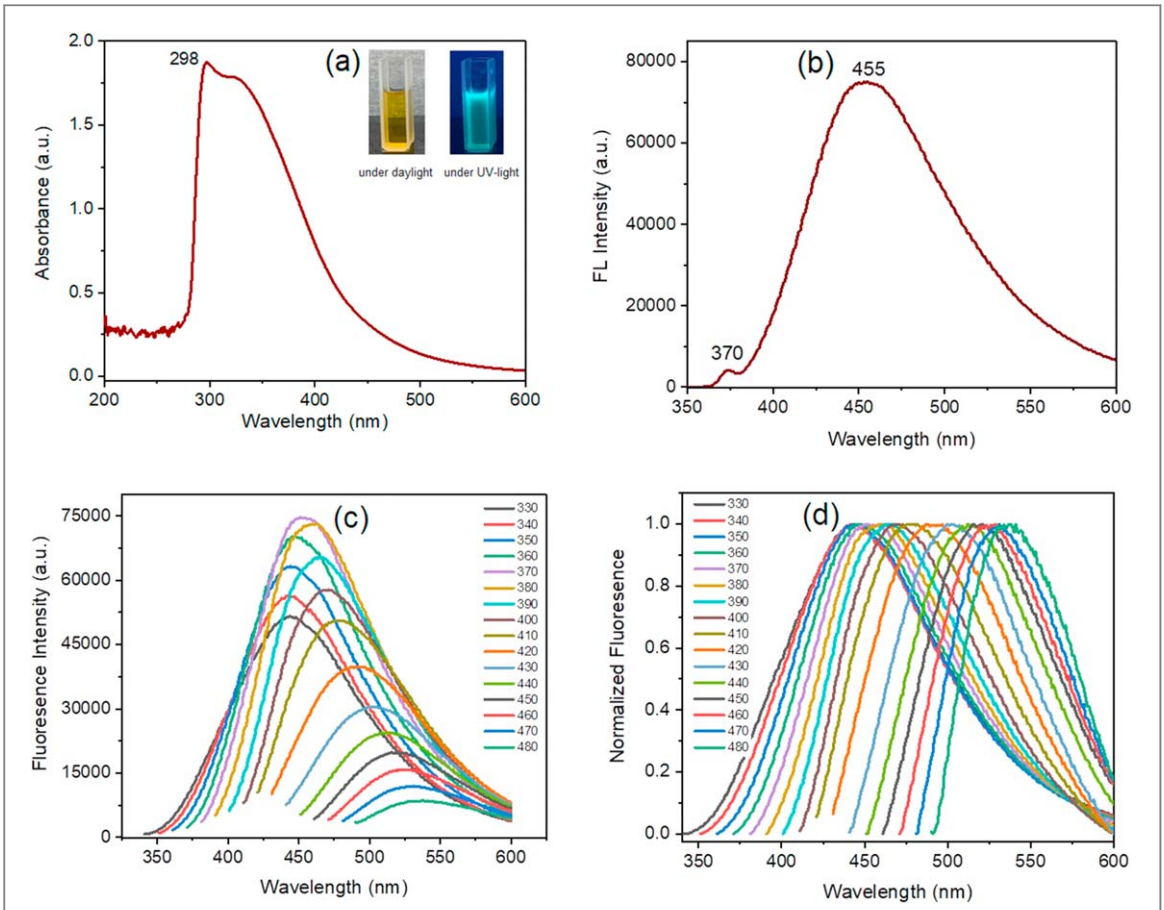

Figure 3. (a) UV–vis absorption spectra, (b) Fluorescence excitation and emission spectra, (c) Variation in fluorescence emission intensity with changes in excitation wavelength, (d) Normalized fluorescence emission spectra for the synthesized N-GQDs.

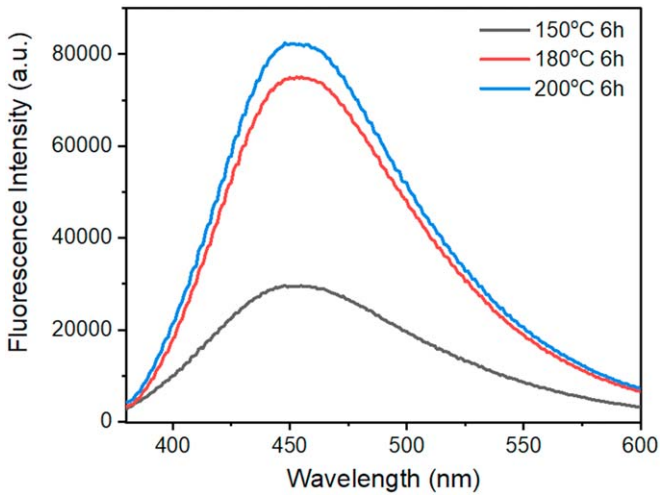

Figure 4. Temperature-dependent fluorescence emission spectra of the N-GQDs were evaluated at near the maximum emission intensity.

carbohydrates and cellulose, transitional compounds may be formed [40]. When grass and nitrogen dopants (EDA) are subjected to high-pressure and high-temperature hydrothermal treatment, smaller precursor molecules are generally transformed into fluorophores [29]. The fluorophores formed during prolonged heating in the hydrothermal treatment may undergo dehydration and polymerization, followed by carbonization, ultimately leading to the formation of N-GQDs [41, 42].

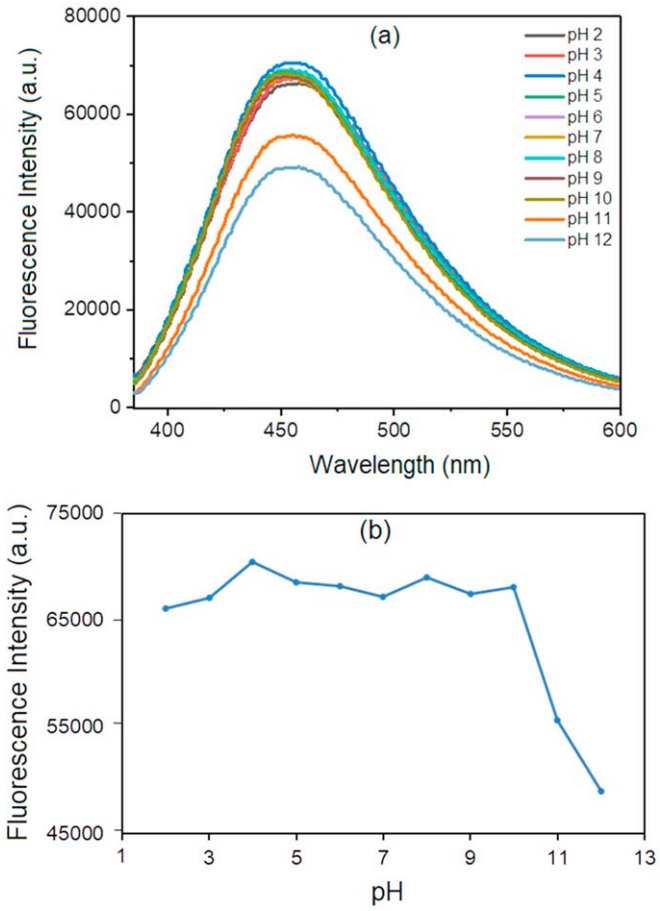

Figure 5. (a) Fluorescence spectra under different pH variations, (b) Fluorescent intensity based on various pH.

3.2. Optical behavior of the N-GQDs

UV–vis absorption and fluorescence spectroscopy were employed to assess the optical behavior of N-GQDs. The absorbance spectrum of the obtained N-GQDs depicted in figure 3(a) reveals two shoulder peaks around 290–300 and 320–400 nm in the absorption spectrum of N-GQDs. According to Atchudan *et al* (2018), the $\pi \rightarrow \pi^*$ transition bands observed at 298 nm are ascribed to the transition of conjugated aromatic sp^2 domains (C=C and C=N bonds) within the carbon structure [36]. The typical $n \rightarrow \pi^*$ transition observed is a consequence of the existence of the C=O functionality on the surface of N-GQDs, which is responsible for the wide absorbance peak observed in the range of 325 to 370 nm. In inset figure 3(a), the aqueous suspension of N-GQDs is presented in the inset as light-brown in daylight and exhibits bright blue fluorescence when exposed to UV light at 365 nm.

Figure 3(b) displays the fluorescence spectra of the maximum excitation and emission wavelengths of the synthesized N-GQDs, which were observed at 370 and 455 nm respectively. Furthermore, the fluorescence emission spectra of N-GQDs were examined at varying excitation wavelengths with 10 nm intervals as depicted in figure 3(c). Increasing the excitation wavelength by 10 nm, from 330 nm to 480 nm, caused a red-shift of the emission wavelength toward a longer wavelength as seen in figure 3(d), and the intensity steadily declined with subsequent increases in the excitation wavelength. These phenomena are called the excitation-dependent fluorescence responses noticed in the N-GQDs (figure 3(d)). This behavior is ascribed to the occurrence of various surface defects and surface states, as explained in previous studies [2, 7]. The emergence of diverse functional groups (–OH, –COOH, –C=O, and $–NH_2$) on the surface of N-GQDs likely has an impact on their size and results in the emergence of different energy levels [43]. The excitation wavelength-dependent emission spectra indicated that not only the size of the N-GQDs but also the allocation of luminescent centers on each N-GQDs had a significant impact on the fluorescence behavior. The quantum yield of the synthesized N-GQDs was determined to be 26% employing quinine sulfate as a standard.

Here, it is important to note that the fluorescence spectra mentioned above are observed when N-GQDs are synthesized at a hydrothermal temperature of 180 °C. The formation of N-GQDs is highly influenced by the hydrothermal temperature, and as a result, the fluorescence emission spectra of N-GQDs are significantly altered [17]. To illustrate this, figure 4 demonstrates the temperature-dependent changes in the fluorescence

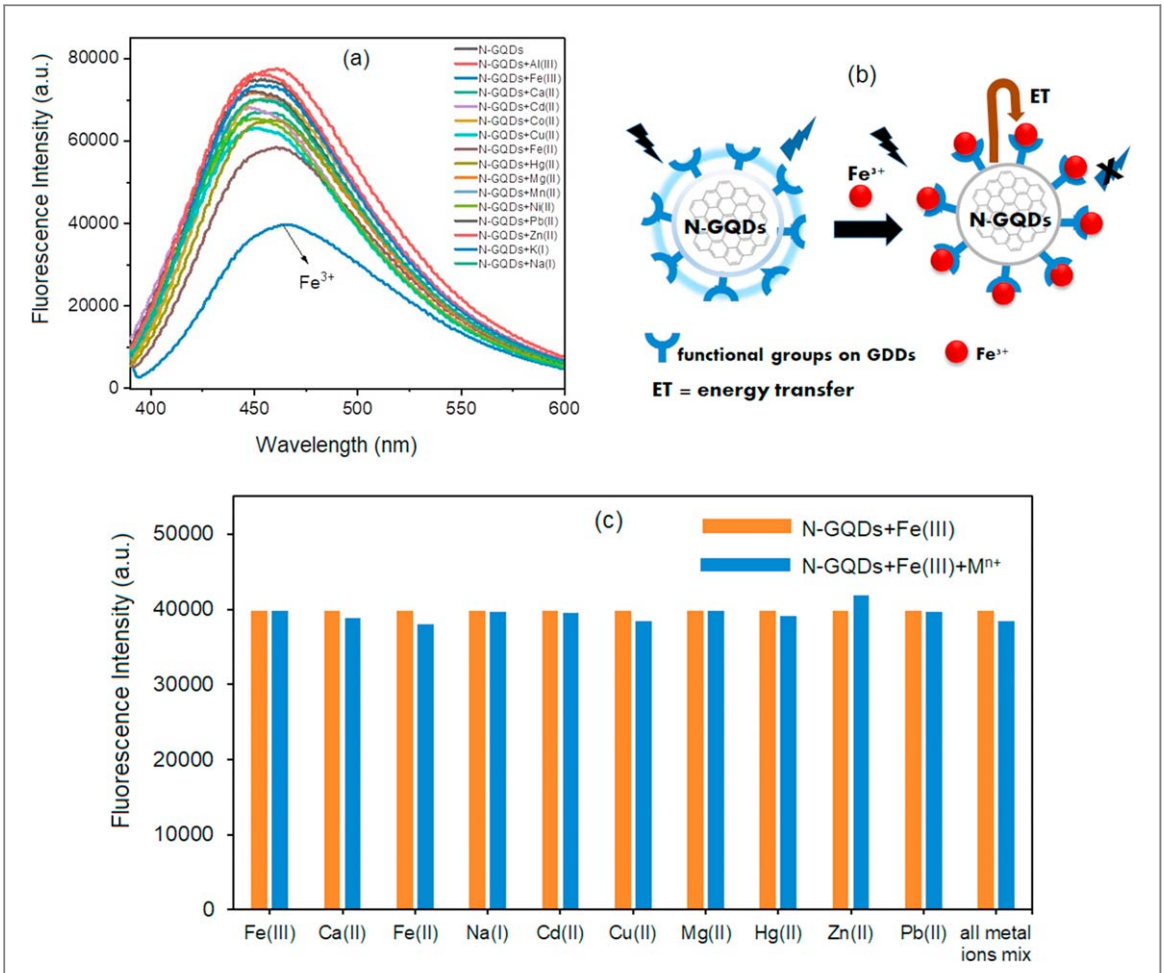

Figure 6. (a) Comparison of the fluorescence intensities of N-GQDs in the existence of diverse metal ions with a 370 nm excitation wavelength, (b) Schematic quenching of N-GQDs under the influence of Fe^{3+}, (c) Interference of the N-GQDs for Fe^{3+} detection in the presence of other metal ions (M^{n+}).

emission spectra of N-GQDs, specifically near the peak emission intensity. It is evident that an increase in the hydrothermal temperature greatly enhances the maximum emission intensity. However, the enhancement in the maximum emission intensity does not correspond to the change in emission wavelength. For instance, at a hydrothermal temperature of 150 °C, the emission wavelength is 451 nm. This wavelength increases to 455 nm at a temperature of 180 °C but decreases to 448 nm at a temperature of 200 °C. The larger emission wavelength at 180 °C indicates a red shift in the emission wavelength, which is more advantageous for sensing applications. Consequently, our subsequent discussion solely focuses on N-GQDs synthesized at a hydrothermal temperature of 180 °C.

3.3. The relationship between pH and N-GQDs fluorescence intensity

The synthesized N-GQDs exhibit surface properties containing hydroxyl, amino, and carbon functional groups, as indicated by ATR-FTIR analysis. The fluorescence intensity of N-GQDs is able to monitor by utilizing these functional groups to study the effect of pH. Figures 5(a), (b) displays the fluorescence intensities of N-GQDs under varying pH values at an excitation wavelength of 370 nm, highlighting the significant influence of pH on N-GQDs fluorescence intensity. As demonstrated in figures 5(a), (b), N-GQDs fluorescence intensity steadily increases and reaches a maximum at a pH of 4 as the pH value rises from 2–4 [8]. Subsequently, a slight variation of the N-GQDs fluorescence intensity occurs at pH ranging from 2 to 10 but significantly decreases at alkaline (pH 11 or 12) conditions. This fluorescence intensity dependent on pH arises due to various factors, including changes in the surface chemistry and structural properties of the N-GQDs [38]. Typically, N-GQDs contain different functional groups on their surface, such as carboxylic acid, hydroxyl groups, and amino groups. These functional groups can undergo protonation or deprotonation depending on the pH of the solution, leading to changes in the surface charge and electronic structure of the N-GQDs, significantly affecting the fluorescence behavior [44, 45]. Under acidic conditions, the carboxyl and hydroxyl groups on the N-GQDs surface form hydrogen bonds through the aggregation of non-covalent bonds. Since the non-radiative rotational relaxation is

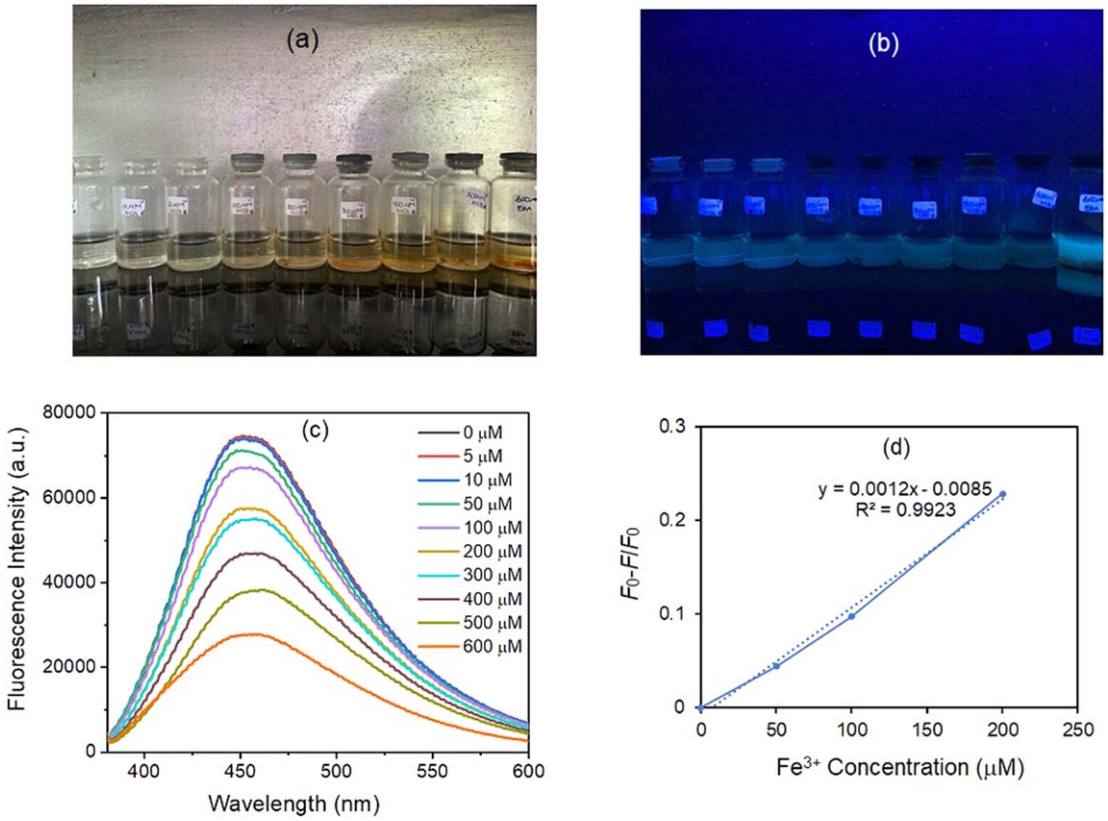

Figure 7. N-GQDs+Fe^{3+} solutions in various concentrations under (a) day-light and (b) UV-light, (c) The emission spectra of N-GQDs under different concentrations of Fe^{3+} ions, and (d) Corresponding linear plot (F_0 and F are the fluorescence intensities of N-GQDs without and with Fe^{3+} ions).

reduced by the formation of a rigid molecular conformation, this leads to an increase in the fluorescence intensity of the N-GQDs as indicated in figures 5(a), (b). Conversely, in alkaline solutions, the oxygen functional groups on the N-GQDs surface are in a deprotonated state, appearing as isolated particles, thus resulting in a decrease in the fluorescence intensity of the N-GQDs [46].

In summary, the pH-responsive fluorescent properties of N-GQDs can be assigned to the functional groups present on their surface. The fluorescence quenching of N-GQDs occurs primarily as a consequence of N-GQDs aggregation particles when their surface functional groups become protonated. Consequently, N-GQDs can also be harnessed as pH probes owing to their sensitivity to pH.

3.4. Detection of Fe^{3+}

The fluorescent characteristics of the prepared N-GQDs were employed as a sensor platform to identify a variety of metal ions in water solutions. The intensity of fluorescence emitted by the solution of N-GQDs changed upon the introduction of metal ions for instance Na^{+}, Mg^{2+}, Al^{3+}, K^{+}, Ca^{2+}, Mn^{2+}, Fe^{2+}, Fe^{3+}, Co^{2+}, Ni^{2+}, Cu^{2+}, Zn^{2+}, Cd^{2+}, Hg^{2+}, and Pb^{2+} at a concentration of 600 μM using a 370 nm excitation wavelength. The fluorescence signals of N-GQDs were quenched the most in the context of Fe^{3+} ions at the same concentrations. The coordination of metal ions on the N-GQDs surface showed different fluorescence emission intensities at the same excitation wavelength of 370 nm, suggesting metal affinity. The quenching effect of N-GQDs was observed with the existence of diverse metal ions as revealed in figure 6(a).

The fluorescence intensity of N-GQDs was detected to be varying with the introduction of different metal ions (see figure 6(a)). Based on the results, Fe^{3+} ions showed a remarkable decrease in the fluorescence intensity of N-GQDs, indicating that the N-GQDs is selective to the Fe^{3+} ions. The decrease in the fluorescence intensity of N-GQDs under the presence of the Fe^{3+} ions might be explained by the strong affinity between Fe^{3+} ions and N-GQDs [29]. The introduction of Fe^{3+} ions resulted in an immediate and effective quenching of N-GQDs. This phenomenon can be explained due to the intense affinity amongst the functional groups of N-GQDs and Fe^{3+} ions. This interaction leads to the assembly of Fe^{3+}-N-GQDs coordination structure, which facilitates efficiency energy transfer and subsequent fluorescence intensity in the existence of metal ions, the quenching mechanism can be seen in figure 6(b).

Table 1. A comparison between the current study and previously reported research on the detection of Fe^{3+} ions using biomass-based carbon nanodots synthesized by hydrothermal approach.

Material	Precursors	Maximum Excitation (nm)	QY (%)	Linier Range (μM)	LOD (μM)	References
GQDs	Cane molasses	360 380	10.44	0–60	5.77	[47]
PEG-GQDs			21.32			
N-CQDs	Rice residue	360	23.48	3.32–32.26	0.7462	[48]
GQDs	Black tea bags	—	~26%	0.1–100	0.29 ± 0.4	[49]
N-GQDs	*Pennisetum purpureum*	370	~26%	0–600	0.06	This work

To further validate the selectivity of Fe^{3+} ions, we present in figure 6(c) the fluorescence intensity of N-GQDs+Fe^{3+} when other metal ions are present. The results demonstrate that the addition of these other ions has minimal interference or impact on the fluorescence intensity of N-GQDs+Fe^{3+}. Despite the presence of various other metal ions, the decrease in fluorescence intensity of N-GQDs caused by the quenching process of Fe^{3+} ions remain relatively consistent. Hence, it can be concluded that N-GQDs exhibit high selectivity towards Fe^{3+} ions due to a distinct fluorescence quenching mechanism elucidated in figure 6(b).

The limit of detection (LOD) of N-GQDs was evaluated by examining the fluorescence intensities in the appearance of varying concentrations of Fe^{3+} ions. The N-GQDs+Fe^{3+} solutions in various concentrations under day-light and UV-light are schematically shown in figures 7(a), (b), respectively. As demonstrated in figure 7(c), the concentration-dependent decrease in fluorescence intensity was noticed as the Fe^{3+} ions concentration was raised incrementally from 0 to 600 μM (see figures 7(a)–(b), owing to the complete complexation between N-GQDs and Fe^{3+} ions, which results from an increase in hydroxyl, amine, and carboxylic functional groups on the surface and charge or electron transfer within the complex, as reported in reference [47–49]. The $(F_0\text{-}F)/F_0$ plot in figure 7(d) indicates a relatively fast quenching of Fe^{3+} ions, demonstrating a strong linear correlation at both inadequate and excessive concentrations. Here, F_0 and F denote fluorescence intensity in the absence and the presence of metal ions, respectively. The LOD for Fe^{3+} detection was calculated to be 69.14 nM, with a strong linear correlation observed between $(F_0\text{-}F)/F_0$ and the 0–200 μM concentration of Fe^{3+} ion, as evidenced by the R^2 value of 0.9923.

The remarkable fluorescence, exceptional purity, high water solubility, and precise surface modification of these N-GQDs contribute to their remarkably low LOD for detecting Fe^{3+}. The findings of this study demonstrate the outstanding sensitivity of the N-GQDs-based sensor in identifying Fe^{3+} ions. In comparison to the previous findings, as indicated in table 1, the synthesized N-GQDs demonstrate a superior limit of detection (LOD). With these advantages, we are confident that these N-GQDs will prove to be a reliable and effective tool for detecting Fe^{3+} in sensing applications.

4. Conclusions

The hydrothermal method was utilized to synthesize N-GQDs, employing *Pennisetum purpureum* as the carbon precursor and EDA as the nitrogen source, without the requirement of any organic solvents. The resulting N-GQDs exhibit blue emission and possess excellent pH stability in the range of pH 3–10. Furthermore, these N-GQDs feature high sensitivity towards nitrogen atoms trapped on their surface and can specifically detect Fe^{3+} among various types of metal ions. A strong linear correlation is observed between the fluorescence intensity ratio $(F_0\text{-}F)/F_0$ and concentration within the range 0–600 μM, with a LOD of 60 nM. It is proposed that the quenching mechanism involves the coordinated bond formation between Fe^{3+} ions and the oxygen/nitrogen-containing functional groups attached to the surface of N-GQDs. The N-GQDs that were synthesized exhibit excellent fluorescence quantum yield of 26%, making fluorescent probe becomes promising for Fe^{3+} ions detection in water-based solutions.

Acknowledgments

The authors acknowledge Kemdikbud Ristek Indonesia for PDD 2022 research grant (089/E5/PG.02.00/PT/2022; 1914/UN1/DITLIT/Dit-Lit/PT.01.03/2022).

Data availability statement

The data cannot be made publicly available upon publication because they contain commercially sensitive information. The data that support the findings of this study are available upon reasonable request from the authors.

ORCID iDs

Indriana Kartini https://orcid.org/0000-0001-9558-8094

References

[1] Sadasivuni K K, Ponnamma D, Thomas S and Grohens Y 2014 Evolution from graphite to graphene elastomer composites *Prog. Polym. Sci.* **39** 749–80
[2] Kumar Y R, Deshmukh K, Sadasivuni K K and Pasha S K K 2020 Graphene quantum dot based materials for sensing, bio-imaging and energy storage applications: a review *RSC Adv.* **10** 23861–98
[3] Elvati P, Baumeister E and Violi A 2017 Graphene quantum dots: effect of size, composition and curvature on their assembly *RSC Adv.* **7** 17704–10
[4] Zhu X, Zhang Z, Xue Z, Huang C, Shan Y, Liu C, Qin X, Yang W, Chen X and Wang T 2017 Understanding the selective detection of Fe3+ based on graphene quantum dots as fluorescent probes: the Ksp of a metal hydroxide-assisted mechanism *Anal. Chem.* **89** 12054–8
[5] Sangam S *et al* 2018 Sustainable synthesis of single crystalline sulphur-doped graphene quantum dots for bioimaging and beyond *Green Chem.* **20** 4245–59
[6] Zhao C *et al* 2020 Synthesis of graphene quantum dots and their applications in drug delivery *J. Nanobiotechnol* **18** 142–32
[7] Abbas A, Tabish T A, Bull S J, Lim T M and Phan A N 2020 High yield synthesis of graphene quantum dots from biomass waste as a highly selective probe for Fe3+ sensing *Sci Rep.* **10** 1–16
[8] Nguyen K G, Baragau I A, Gromicova R, Nicolaev A, Thomson S A J, Rennie A, Power N P, Sajjad M T and Kellici S 2022 Investigating the effect of N-doping on carbon quantum dots structure, optical properties and metal ion screening *Sci Rep.* **12** 1–12
[9] Danial W H, Abdullah M, Abu Bakar M A, Yunos M S, Ibrahim A R, Iqbal A and Adnan N N 2022 The valorisation of grass waste for the green synthesis of graphene quantum dots for nonlinear optical applications *Opt. Mater. (Amst).* **132** 112853
[10] Strezov V, Evans T J and Hayman C 2008 Thermal conversion of elephant grass (Pennisetum Purpureum Schum) to bio-gas, bio-oil and charcoal *Bioresour. Technol.* **99** 8394–9
[11] Picard M, Thakur S, Misra M and Mohanty A K 2019 Miscanthus grass-derived carbon dots to selectively detect Fe3+ ions *RSC Adv.* **9** 8628–37
[12] Sabet M and Mahdavi K 2019 Green synthesis of high photoluminescence nitrogen-doped carbon quantum dots from grass via a simple hydrothermal method for removing organic and inorganic water pollutions *Appl. Surf. Sci.* **463** 283–91
[13] Liu S, Tian J, Wang L, Zhang Y, Qin X, Luo Y, Asiri A M, Al-Youbi A O and Sun X 2012 Hydrothermal treatment of grass: a low-cost, green route to nitrogen-doped, carbon-rich, photoluminescent polymer nanodots as an effective fluorescent sensing platform for label-free detection of Cu(II) ions *Adv. Mater.* **24** 2037–41
[14] Li L S, Jiao X Y, Zhang Y, Cheng C, Huang K and Xu L 2018 Green synthesis of fluorescent carbon dots from Hongcaitai for selective detection of hypochlorite and mercuric ions and cell imaging *Sensors Actuators, B Chem.* **263** 426–35
[15] Sun C, Zhang Y, Wang P, Yang Y, Wang Y, Xu J, Wang Y and Yu W W 2016 Synthesis of nitrogen and sulfur co-doped carbon dots from garlic for selective detection of Fe3+ *Nanoscale Res. Lett.* **11** 1–9
[16] Liu Y, Gong X, Dong W, Zhou R, Shuang S and Dong C 2018 Nitrogen and phosphorus dual-doped carbon dots as a label-free sensor for curcumin determination in real sample and cellular imaging *Talanta* **183** 61–9
[17] Ru G J, Xin Q, Rui J X and Shah H 2019 Single precursor-based luminescent nitrogen-doped carbon dots and their application for iron (III) sensing *Arab. J. Chem.* **12** 1083–91
[18] Atchudan R, Edison T N J I, Aseer K R, Perumal S, Karthik N and Lee Y R 2018 Highly fluorescent nitrogen-doped carbon dots derived from Phyllanthus acidus utilized as a fluorescent probe for label-free selective detection of Fe3+ ions, live cell imaging and fluorescent ink *Biosens. Bioelectron.* **99** 303–11
[19] Yang H L, Bai L F, Geng Z R, Chen H, Xu L T, Xie Y C, Wang D J, Gu H W and Wang X M 2023 Carbon quantum dots: preparation, optical properties, and biomedical applications *Mater. Today Adv.* **18** 100376
[20] Kadian S and Manik G 2020 Sulfur doped graphene quantum dots as a potential sensitive fluorescent probe for the detection of quercetin *Food Chem.* **317** 126457
[21] Wang Z, Chen D, Gu B, Gao B, Wang T, Guo Q and Wang G 2020 Biomass-derived nitrogen doped graphene quantum dots with color-tunable emission for sensing, fluorescence ink and multicolor cell imaging *Spectrochim. Acta - Part A Mol. Biomol. Spectrosc.* **227** 117671
[22] Martins E C, Santana E R and Spinelli A 2023 Nitrogen and sulfur co-doped graphene quantum dot-modified electrode for monitoring of multivitamins in energy drinks *Talanta* **252** 123836
[23] Esteves M, Mombrú D, Romero M, Fernández-werner L, Faccio R and Mombrú A W 2023 The structural , optical and electrical properties of sodium titanate nanotubes sensitized with nitrogen / sulfur co-doped graphene quantum dots as potential materials for quantum dots sensitized solar cells *Mater. Today Electron.* **3** 100029
[24] Manioudakis J, Victoria F, Thompson C A, Brown L, Movsum M, Lucifero R and Naccache R 2019 Effects of nitrogen-doping on the photophysical properties of carbon dots *J. Mater. Chem.* C **7** 853–62
[25] Baker S N and Baker G A 2010 Luminescent Carbon Nanodots : Emergent Nanolights Angewandte *Angewandte Chemie International Edition* **49** 6726–44
[26] Howe J Y, Rawn C J, Jones L E and Ow H 2003 Improved crystallographic data for graphite *Powder Diffr.* **18** 150–4
[27] Robertson A W and Warner J H 2011 Hexagonal single crystal domains of few-layer graphene on copper foils *Nano Lett.* **11** 1182–9
[28] Hyun K and Saito N 2017 The solution plasma process for heteroatom-carbon nanosheets: the role of precursors *Sci Rep.* **7** 1–9

[29] Edison T N J I, Atchudan R, Shim J J, Kalimuthu S, Ahn B C and Lee Y R 2016 Turn-off fluorescence sensor for the detection of ferric ion in water using green synthesized N-doped carbon dots and its bio-imaging *J. Photochem. Photobiol. B Biol.* **158** 235–42
[30] Li L, Li L, Chen C P and Cui F 2017 Green synthesis of nitrogen-doped carbon dots from ginkgo fruits and the application in cell imaging *Inorg. Chem. Commun.* **86** 227–31
[31] Sun F, Ghosh H, Tan Z and Sivoththaman S 2023 Top-down synthesis and enhancing device adaptability of graphene quantum dots *Nanotechnology* **34** 185061–7
[32] Krishnaiah P, Atchudan R, Perumal S, Salama E S, Lee Y R and Jeon B H 2022 Utilization of waste biomass of Poa pratensis for green synthesis of n-doped carbon dots and its application in detection of Mn2+ and Fe3 *Chemosphere.* **286** 131764
[33] Kaniyoor A and Ramaprabhu S 2012 A Raman spectroscopic investigation of graphite oxide derived graphene *AIP Adv.* **2** 032183–13
[34] Yoshikawa M, Nagai N, Matsuki M, Fukuda H, Katagiri G, Ishida H, Ishitani A and Nagai I 1992 Raman scattering by sp2 amorphous carbons *Phys. Rev.* B **46** 7169
[35] Baweja H and Jeet K 2019 Economical and green synthesis of graphene and carbon quantum dots from agricultural waste *Mater. Res. Express* **6** 0850g8
[36] Atchudan R, Edison T N J I, Aseer K R, Perumal S and Lee Y R 2018 Hydrothermal conversion of Magnolia liliiflora into nitrogen-doped carbon dots as an effective turn-off fluorescence sensing, multi-colour cell imaging and fluorescent ink *Colloids Surfaces B Biointerfaces.* **169** 321–8
[37] Wen J, Li N, Li D, Zhang M, Lin Y, Liu Z, Lin X and Shui L 2021 Cesium-doped graphene quantum dots as ratiometric fluorescence sensors for blood glucose detection *ACS Appl. Nano Mater.* **4** 8437–46
[38] Wu P, Li W, Wu Q, Liu Y and Liu S 2017 Hydrothermal synthesis of nitrogen-doped carbon quantum dots from microcrystalline cellulose for the detection of Fe3+ ions in an acidic environment *RSC Adv.* **7** 44144–53
[39] Chen Y, Sun X, Pan W, Yu G and Wang J 2020 Fe3+-sensitive carbon dots for detection of Fe3+ in aqueous solution and intracellular imaging of Fe3+ inside fungal cells *Front. Chem.* **7** 1–9
[40] Wang M, Wan Y, Zhang K, Fu Q, Wang L, Zeng J, Xia Z and Gao D 2019 Green synthesis of carbon dots using the flowers of osmanthus fragrans (Thunb.) Lour. as precursors: application in Fe 3+ and ascorbic acid determination and cell imaging *Anal. Bioanal. Chem.* **411** 2715–27
[41] Roy P, Chen P C, Periasamy A P, Chen Y N and Chang H T 2015 Photoluminescent carbon nanodots: Synthesis, physicochemical properties and analytical applications *Mater. Today* **18** 447–58
[42] Malavika J P, Shobana C, Ragupathi M, Kumar P, Lee Y S, Govarthanan M and Selvan R K 2021 A sustainable green synthesis of functionalized biocompatible carbon quantum dots from aloe barbadensis miller and its multifunctional applications *Environ. Res.* **200** 111414
[43] Yao Q, Wu H, Jin Y, Wang C, Zhang R, Lin Y, Wu S and Hu Y 2022 One-pot synthesis of fluorescent nitrogen-doped graphene quantum dots for portable detection of iron ion *Curr. Appl Phys.* **41** 191–9
[44] Bhattacharyya S, Ehrat F, Urban P, Teves R, Wyrwich R, Döblinger M, Feldmann J, Urban A S and Stolarczyk J K 2017 Effect of nitrogen atom positioning on the trade-off between emissive and photocatalytic properties of carbon dots *Nat. Commun.* **8** 1–9
[45] Liu C, Zhang F, Hu J, Gao W and Zhang M 2021 A mini review on pH-sensitive photoluminescence in carbon nanodots *Front. Chem.* **8** 1–9
[46] Li C, Zhang X, Zhang W, Qin X and Zhu C 2019 Carbon quantum dots derived from pure solvent tetrahydrofuran as a fluorescent probe to detect pH and silver ion *J. Photochem. Photobiol. A Chem.* **382** 111981
[47] Lou Y, Ji J, Qin A, Liao L, Li Z, Chen S, Zhang K and Ou J 2020 Cane molasses graphene quantum dots passivated by PEG functionalization for detection of metal ions *ACS Omega.* **5** 6763–72
[48] Qi H *et al* 2019 Biomass-derived nitrogen-doped carbon quantum dots: highly selective fluorescent probe for detecting Fe 3+ ions and tetracyclines *J. Colloid Interface Sci.* **539** 332–41
[49] Abbas A, Liang Q, Abbas S, Liaqat M, Rubab S and Tabish T A 2022 Eco-friendly sustainable synthesis of graphene quantum dots from biowaste as a highly selective sensor *Nanomaterials.* **12** 1–13